ISSN 2616-5775 Vol. 8, Issue 8: 1-7, DOI: 10.25236/AJCIS.2025.080801

Research on Rapid Iris Localization Algorithm Based on Projection Analysis

Nan Liu

School of Mechanical and Electrical Engineering and Automation, Xiamen University Tan Kah Kee College, Zhangzhou, China
liunan@xujc.com

Abstract: *With the accelerated advancement of global digitalization, information interconnectivity has become a fundamental characteristic of modern society. During this transformative process, the security vulnerabilities of traditional identity authentication systems have become increasingly prominent: current systems primarily rely on physical credentials and multi-factor password mechanisms. These static verification methods not only suffer from inherent weaknesses such as susceptibility to loss and forgery but may also lead to severe personal privacy breaches and societal security risks due to information leakage. In the face of increasingly sophisticated cybersecurity threats, the development of novel identity authentication technologies has become an urgent necessity for ensuring digital security. As a critical direction in identity authentication, biometric technology verifies identity by analyzing individuals' unique physiological or behavioral characteristics. Among these, iris recognition technology demonstrates significant technical superiority and broad application prospects due to its liveness detection capability, contactless acquisition, high uniqueness, long-term stability, and inherent anti-counterfeiting properties. However, existing iris recognition technologies still face major challenges in practical applications: not all scenarios can provide sufficient computational resources or deployment space. To address this critical issue, this study innovatively proposes a longitudinal gray-scale integration-based iris segmentation method. This approach can operate efficiently on miniaturized PCs or embedded processors while achieving precise center localization, thereby providing a reliable foundation for subsequent iris texture recognition.*

Keywords: *Machine Vision, Gray-Scale Integration, Iris Segmentation, Hamming Distance, Iris Matching*

1. Related work

Since the 1960s, biometric technology has evolved significantly and achieved commercial application by the 1990s[1]. Biometric characteristics can be classified into physiological and behavioral features, which have become a secure and reliable means of identity authentication due to their uniqueness and resistance to counterfeiting. Among these, iris recognition is considered one of the most secure biometric technologies owing to its high accuracy, contactless operation, and strong anti-spoofing capabilities, finding widespread applications in identity verification, access control systems, and related fields[2-3].

However, the key technical challenge lies in iris localization, primarily affected by the following factors: physiological interference, imaging conditions, user cooperation, and hardware limitations of capture devices[4]. Current iris localization methods are mainly divided into two categories: traditional vision algorithms and deep learning approaches[5]. Although neural networks demonstrate superior accuracy, their reliance on large-scale training data and high computational costs make them difficult to deploy efficiently on low-power devices[6]. Therefore, traditional vision methods remain competitive in scenarios demanding real-time performance or operating under resource constraints. Future research will focus on developing iris recognition algorithms that simultaneously achieve high precision, low power consumption, and strong robustness[7].

In the field of iris segmentation, Daugman's classical algorithm employs differential integral operators to achieve precise localization, but it suffers from a cubic time complexity bottleneck[8] Subsequently, Wildes proposed an improved approach that combines edge detection in raw images with a parameter-space voting mechanism based on circular Hough transform, optimizing time complexity while maintaining localization accuracy[9]. Huang's team introduced a multi-scale hierarchical search strategy, effectively reducing localization time through a progressive precision enhancement

ISSN 2616-5775 Vol. 8, Issue 8: 1-7, DOI: 10.25236/AJCIS.2025.080801

mechanism[10]. Liu's team explored the application of the Canny edge detector in accelerating Hough transform-based localization[11] Sung's team proposed a bisection method for inner iris boundary localization, combined with histogram equalization and statistical feature analysis to construct the outer contour[12]. Feng's team developed an improved solution targeting the performance limitations of traditional iris segmentation algorithms[13] however, due to high computational complexity, segmentation accuracy significantly degrades in complex scenarios involving eyelid occlusion, lens reflection, or pupil deformation.

2. Principle of Iris Outer Boundary Localization

The longitudinal gray-scale integration method employed in this study operates by preserving a local mask pattern determined relative to the pupil center. The pupil boundary exhibits symmetry about the x-axis, and since the outer iris boundary approximates a concentric circle with the pupil, it inherits this geometric property. As illustrated in Figure 1, the annular outer iris boundary undergoes adaptive thresholding via mean-value processing during cropped iris image analysis. This operation converts the image into a binary format while suppressing transitional zones through black-level assignment.

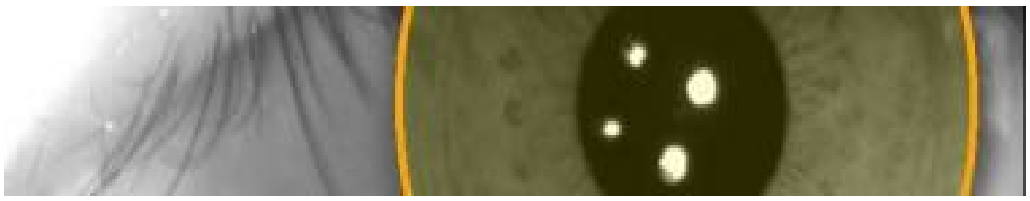

Figure 1 Schematic diagram of the transition zone

The selector subsequently determines the search area. Since the transition zone in this binary image forms an incomplete but still annular structure symmetric about the x-axis, its slope varies progressively along the x-axis. The grayscale integral accumulation reaches its maximum (manifesting as a wave trough) where the slope is steepest (i.e., when the tangent is perpendicular to the x-axis). Based on circular geometry, when setting the circle center as the origin, the maximum slopes occur at the junctions of quadrants I/IV and II/III. The line connecting these two points represents the diameter, allowing determination of the pupil's diameter through their x-coordinate spacing. This data subsequently identifies the circle center and completes segmentation, as illustrated in Figure 2.

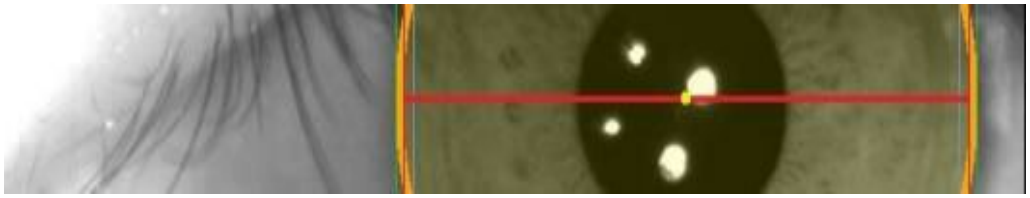

Figure 2 Schematic diagram of longitudinal gradient integral scanning principle

The algorithm employs vertical gradient integration scanning along the x-axis, where distinct vertical lines represent the scanning paths. Given the preserved circular characteristics in the transition zone, the grayscale accumulation during integration progressively increases from the outermost boundary (marked by green lines), reaches a peak at the transition zone center (indicated by red lines), then gradually decreases toward the innermost boundary (denoted by blue lines). The center position of the transition zone is determined by detecting the trough within a specified search range in the gradient histogram.

3. Implementation of Iris Localization and Segmentation Algorithm

3.1 Overall algorithm design

Iris segmentation processing is a technical procedure that accurately extracts the iris and pupil regions by eliminating visual interferences such as the sclera, eyelid occlusion, and light spots. Its essence involves segmenting the pupil edge , segmenting the outer iris boundary, and locating their center points. The segmentation algorithm designed in this paper integrates edge detection, Hough circle transform, dynamic threshold segmentation, grayscale histogram analysis, and other methods. It achieves iris region localization and segmentation in eye images by combining threshold-based extraction with adaptive iris

ISSN 2616-5775 Vol. 8, Issue 8: 1-7, DOI: 10.25236/AJCIS.2025.080801

edge localization. The implementation workflow is illustrated in Figure 3.

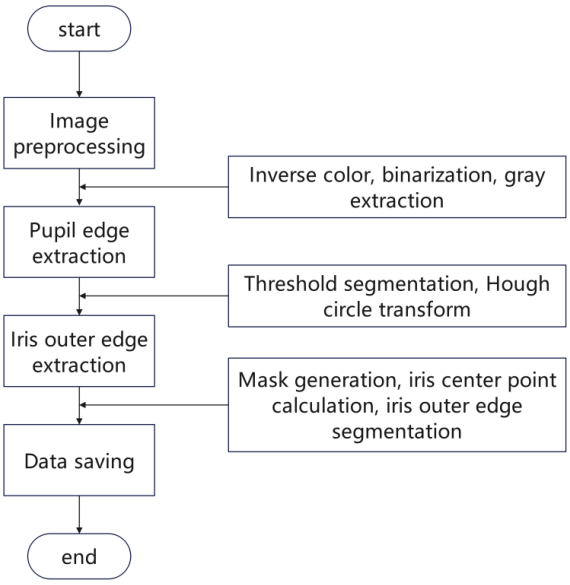

Figure 3 Algorithm implementation flow chart

3.2 Image preprocessing

For more effective extraction of light spots in the pupil area, image inversion followed by binarization processing can directly render the light spots as black void points.

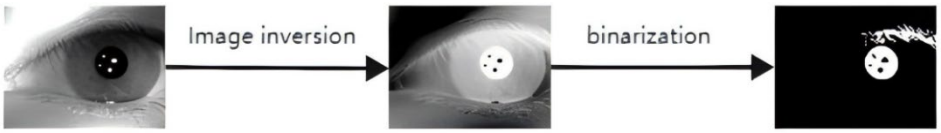

Figure 4 Image inversion and binarization

In the binarized image shown in Figure 4, both the pupil region and eyelash artifacts are visible, with the latter containing fine noise points. The presence of these artifacts may adversely affect subsequent light spot removal. By performing contour detection followed by hole-filling operations on all identified contours, this procedure aims to preliminarily delineate the circular pupil area while simultaneously closing any contained light spot regions.

By performing the Hough circle transform, we can further screen out circular regions that cover the pupil area without interference from other connected regions, as demonstrated in Figure 5.

Figure 5 Hough circle transformation and gray filling

After the above operations, we have initially obtained the pupil boundary, but it is only roughly circular at this stage. By applying the Hough circle transform based on the existing contour, we further refine and accurately determine the pupil region.

3.3 Iris segmentation and extraction algorithm

In the iris segmentation process, the outer iris boundary is located based on the center and radius of the pupil circle, utilizing the property that the pupil and iris circles are approximately concentric[14]. Through the aforementioned steps, we have completed the detection of the pupil boundary and stored its

ISSN 2616-5775 Vol. 8, Issue 8: 1-7, DOI: 10.25236/AJCIS.2025.080801

center coordinates and radius data. Based on this data, since we adopt a grayscale-based approach to locate the outer iris boundary, eyelash interference in the original captured image can significantly affect the grayscale values.

Finally, the edge localization is achieved through vertical grayscale integral projection. A vertical grayscale integral projection is performed on the binary image by calculating the sum of grayscale values for each column. The previously stored pupil center coordinates and radius information are retrieved to classify the search range for the outer iris boundary.

Based on the defined search interval, the integral projection values within this range are extracted. The column indices corresponding to the minimum integral projection values within the left and right intervals are identified and marked on the preprocessed image. These troughs are determined to represent the outer iris boundary.

After obtaining the column positions of the outer iris edges in the horizontal direction (i.e., determining the diameter of the iris circle), we set the pupil center coordinates as (x0, y0). The horizontal coordinates of the outer iris edge columns are designated as p1 (corresponding to the right peak) and p2 (corresponding to the left peak). From these values, we calculate the iris center coordinates I(x1, y1) and radius r1 using the following formulas:

$$\begin{cases} r1 = \frac{p2-p1}{2} \\ x1 = \frac{p2+p1}{2} \\ y1 = y0 \end{cases} \tag{1}$$

Based on Equation 1, the center coordinates and radius corresponding to the outer iris boundary can be calculated. We plot these parameters on the original image and store the resulting data. The final output is shown in Figure 6.

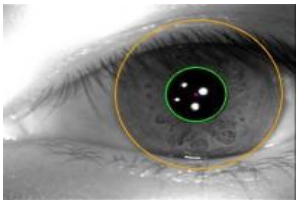

Figure 6 Final result of iris segmentation and pupil segmentation

4. Implementation of iris recognition matching algorithm

After achieving precise localization and segmentation of the iris region in ocular images, the core challenge of the entire iris recognition system lies in efficiently extracting the rich textural features embedded within. Simultaneously, it is essential to select appropriate distance metric functions tailored to different feature extraction methods to accurately quantify their similarities.The phase information extracted by Gabor filters is represented in binary form.

Considering matching efficiency, the Hamming distance is adopted as the similarity metric to conveniently compute the similarity between multiple feature encodings [15]. Originally applied to error-control coding in data transmission, this distance metric measures the number of differing character positions between two strings - i.e., the minimum substitutions required to transform one string into another. For binary strings a and b, their Hamming distance equals the count of '1's in their XOR operation result. The corresponding formula for iris binary codes is as follows:

$$h_{\{R_0,I_m\}} = \operatorname{sgn}_{\{R_0,I_m\}} \iint_{\rho\phi} I(\rho,\theta) e^{-\operatorname{sgn}(\theta_0-\theta)} e^{-(r_0-\theta)\frac{2}{e^2}} \rho d\rho d\theta \tag{2}$$

Here, I(p,θ) represents the iris image. The 2D Gabor filter is formed by the composition of a Gaussian filter and a sinusoidal function. Although this transformation sacrifices some global frequency-domain resolution, it exhibits excellent local spatial responsiveness[16] The output of this filtering method is a complex number. Based on the quadrant distribution characteristics in the complex plane, the transformation results are encoded into four binary combinations: [0 0], [0 1], [1 0], and [1 1]. The corresponding quadrant-to-encoding mapping is illustrated in Figure 7.

ISSN 2616-5775 Vol. 8, Issue 8: 1-7, DOI: 10.25236/AJCIS.2025.080801

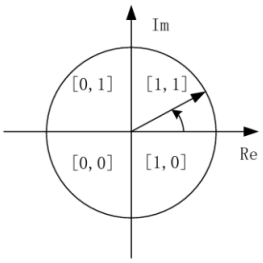

Figure 7 Two dimensional gabor filtering coding map corresponding to different quadrants

We can observe that the essence of this filtering transformation is to convert iris features into binary-code-based feature vectors. This approach is inherently compatible with computer binary computation and facilitates subsequent encoding matching. Denoting the final result as code, its mathematical formulation is presented below:

$$\text{code} = (B1, B2, B3, \ldots Bj \ldots Bk) \tag{3}$$

Thus, depending on which quadrant of the complex plane the result falls into, the corresponding iris feature encoding Bj is determined by the following formula:

$$\begin{cases} h_r > 0, h_i > 0 \\ h_r > 0, h_i < 0 \\ h_r < 0, h_i > 0 \\ h_r < 0, h_i < 0 \end{cases} \Rightarrow \begin{cases} b_j = 11 \\ b_j = 10 \\ b_j = 01 \\ b_j = 00 \end{cases} \tag{4}$$

We conducted similarity detection based on Hamming distance for two distinct databases: one containing the target iris and another excluding it. With a threshold set at 0.35, each test group comprised 100 images. After systematically comparing all images in the test groups against the target image, the visualization results display: (1) the test iris image, (2) its corresponding normalized iris image, and (3) the image with the highest similarity score from the traversal process. These comparative results are presented in Figures 8 and Figures 9, respectively.

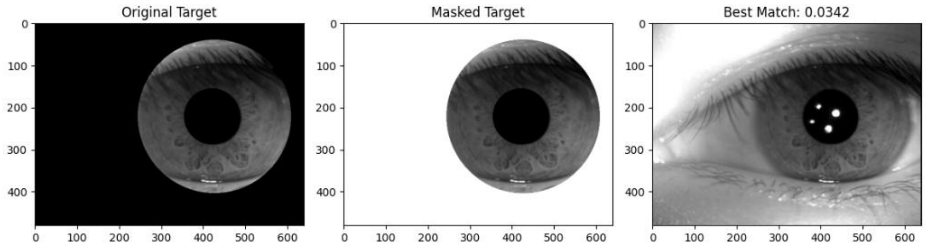

Figure 8 Match to target iris image

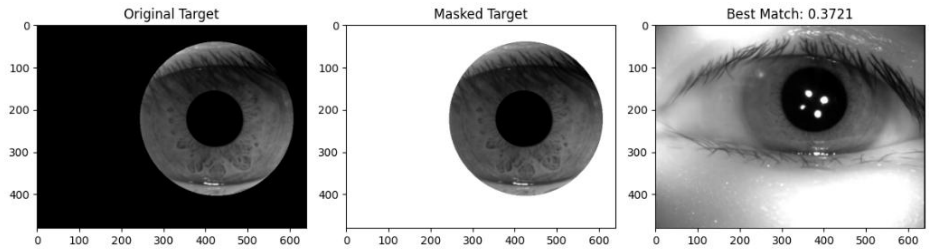

Figure 9 The target iris image is not matched

ISSN 2616-5775 Vol. 8, Issue 8: 1-7, DOI: 10.25236/AJCIS.2025.080801

5. Experimental Process and Results Analysis

5.1 Experimental Process

To validate recognition accuracy, we simulated iris acquisition scenarios using images from the JLU Iris Database developed by the Biometrics and Information Security Research Laboratory at Jilin University. The simulated images replicate raw iris images captured by embedded acquisition systems for accuracy testing. To achieve optimal performance, we fine-tuned specific algorithm parameters. All experimental samples (n=100) were sourced from the JLU-2.0 Iris Database.

The experiment conducted a comparative analysis with the traditional Daugman algorithm, evaluating algorithm performance through accuracy metrics. The comparison results are presented in Table 1.

Table 1 Comparison table of accuracy between this algorithm and traditional Daugman algorithm

Serial Number	name	ACC(%)
1	Daugman	93
2	Ours	99

5.2 Experimental Process

To validate the effectiveness of the image preprocessing stage, this section specifically designs an ablation experiment targeting this module. We perform iris localization and segmentation on both preprocessed and non-preprocessed images, then compare their accuracy. For intuitive demonstration, we intentionally select images with significant interference for comparison. The comparative results with/without preprocessing are shown in Figure 10.

Figure 10 Preprocessed (left) vs. raw (right) image contour extraction comparison

As observed, the non-preprocessed images yield inaccurate results when performing Hough circle transform for contour detection. We randomly selected 100 images and divided them into two groups (with/without preprocessing) for localization and segmentation. The accuracy comparison results are presented in Table 2.

Table 2 Comparison table of accuracy between this algorithm and traditional Daugman algorithm

Serial Number	Pretreatment	ACC(%)
1	Yes	99
2	No	94

The results demonstrate that the preprocessing stage significantly improves localization accuracy. Through verification, we found that non-preprocessed images achieving accurate localization typically contained concentrated highlight regions that did not intersect with pupil boundaries. Conversely, localization failures occurred when highlights approached, intersected, or overlapped with pupil boundaries, thereby disrupting the Hough circle transform's voting accuracy. Preprocessing effectively eliminates this interference through grayscale inpainting, enabling consistent and accurate localization and segmentation.

6. Conclusion

Experimental results demonstrate that compared to conventional methods, the proposed approach exhibits superior adaptability to various environmental interferences (e.g., eyelashes, light spots). Additionally, a Gaussian-weighted method for generating mask images is introduced to accommodate gradually varying illumination in captured images, further enhancing usability.

In summary, the proposed segmentation algorithm combines dynamic threshold extraction with iris edge localization through grayscale integration. It leverages the relatively easier-to-locate pupil edge via Hough circle transform for precise initial positioning, which subsequently facilitates indirect calculation

ISSN 2616-5775 Vol. 8, Issue 8: 1-7, DOI: 10.25236/AJCIS.2025.080801

of the iris center through grayscale integration of both iris edges.

To address potential Hough transform inaccuracies caused by edge light spots, a preprocessing grayscale inpainting technique was implemented. Furthermore, a physiologically constrained classifier based on pupil information effectively mitigates false peaks/valleys caused by excessive iris search ranges. These solutions collectively ensure both accuracy and generalizability.

Acknowledgments

The study was funded by the Xiamen University Tan KahKee College (YM2021L03)

References

[1] Brückner R,Batschelet E,Hugenschmidt F.The Basel longitudinal study on aging (1955-1978). Ophthalmo-gerontological research results.[J]. Documenta ophthalmologica. Advances in ophthalmology, 1986,64(3):235- 310.

[2] Mehrotra Hunny, Vatsa Mayank, Singh Richa, Majhi Banshidhar. Does iris change over time?[J]. PloS one,2013,8(11).

[3] Li Kai. Application of Iris Recognition Technology in Mobile Terminal Field[J]. Network Security Technology & Application, 2015, 000(003): 84-86.

[4] Rathnayake R, Madhushan N, Jeeva A, et al. Real-Time Multi-Spectral Iris Extraction in Diversified Eye Images Utilizing Convolutional Neural Networks[J]. IEEE Access, 2024, 12: 93283-93293.

[5] Gao R, Bourlai T. On designing a swiniris transformer based iris recognition system[J]. IEEE Access, 2024, 12: 30723-30737.

[6] Kulkarni V V, Hatture S M, Karchi R P, et al. IRIS and face-based multimodal biometrics systems[C]//International Conference on Data Analytics & Learning. Singapore: Springer Nature Singapore, 2022: 31-47.

[7] Prabhu R, Nagarajan R. ANFFractalNet: Adaptive neuro-fuzzy FractalNet for iris recognition[J]. Biomedical Signal Processing and Control, 2025, 108: 107984.

[8] Daugman J. The importance of being random: statistical principles of iris recognition [J]. Pattern Recogn,2003,36:279-291.

[9] Wildes R P. Iris recognition: an emerging biometric technology[J]. Proceedings of the IEEE, 2002, 85(9): 1348-1363.

[10] Huang Y P,Luo S W,Chen E Y.An efficient iris recognition system[C]. In: International Conference on Machine Learning & Cybernetics.IEEE,2002:450-454.

[11] Liu Y,Yuan S,ZhuX,Cui Q.A practical iris acquisition system and a fast edgeslocating algorithm in iris recognition[C].In:20th lEEE Conference on Instrumentation and Measurement Technology, 2003: 166-168.

[12] Sung H,Lim J,Park J,Lee Y.Iris recognition using collarette boundary localization[C]. In:17th Interational Conference on Pattern Recognition,2004:857-860.

[13] Feng X,Fang C,DingX,WuY.Iris localization with dual coarse-to-finestrategyl[C].In:18th International Conference on Pattern Recognition,2006:553-55

[14] Nitin K. Mahadeo,Andrew P. Papliński,Sid Ray.Model-based pupil and iris localization[C].IEEE The 2012 International Joint Conference on Neural Networks (IJCNN),2012:1427-1433.

[15] Jayalakshmi S,Sundaresan M,IEEE.A survye on iris segmentation methods[M].New York:IEEE, 2013.

[16] Arts L P A, Van den Broek E L. The fast continuous wavelet transformation (fCWT) for real-time, high-quality, noise-resistant time–frequency analysis[J]. Nature Computational Science, 2022, 2(1): 47-58.